HOKKAIDO UNIVERSITY

Title	Morphology-controlled synthesis of sunlight-driven plasmonic photocatalysts Ag@AgX (X = Cl, Br) with graphene oxide template
Author(s)	Wang, Yanqing; Sun, Ling; Fugetsu, Bunshi
Description	First published online 15 Aug 2013
Citation	Journal of Materials Chemistry A, 1(40), 12536-12544 https://doi.org/10.1039/c3ta12893h
Issue Date	2013-10-28
Doc URL	https://hdl.handle.net/2115/56793
Type	journal article
File Information	JMC-2013-06-11-revise.pdf



Hokkaido University Collection of Scholarly and Academic Papers : HUSCAP

Journal Name

Dynamic Article Links ►

Cite this: DOI: 10.1039/c0xx00000x

www.rsc.org/xxxxxx

ARTICLE TYPE

Morphology-controlled synthesis of sunlight-driven plasmonic photocatalysts Ag@AgX (X=Cl, Br) with graphene oxide template

Yanqing Wang,* Ling Sun and Bunshi Fugetsu

Received (in XXX, XXX) Xth XXXXXXXXX 20XX, Accepted Xth XXXXXXXXX 20XX

DOI: 10.1039/b000000x

Novel cubic Ag@AgX@Graphene (X=Cl, Br) nanocomposites are facilely manipulated by means of a graphene oxide (GO) sheets-assisted assembly protocol, where GO sheets act as amphiphilic template for hetero-growth of AgX nanoparticles. A morphology transformation of AgX nanoparticles from sphere to cube-like was accomplished by involving GO. With a further UV irradiation, the reduction of GO to graphene and the generation of Ag nanocrystals on AgX occur simultaneously. We have demonstrated that thus-produced Ag@AgX@Graphene nanocomposites could be employed as stable plasmonic photocatalysts to decompose acridine orange as a typical dye pollutant under sunlight irradiation. Compared with the bare quasi-spherical Ag@AgX, such graphene-interfaced cubic Ag@AgX nanocomposites display distinctly higher adsorptive capacity, smaller crystal size and reinforced electron-hole pair separation owing to the interfacial contact between Ag@AgX and graphene sheets components, resulting in an enhanced photocatalytic decomposition performance. This investigation provides new possibilities for the development of morphology-controlled plasmonic photocatalysts and facilitates their practical application in environmental issues.

Introduction

Semiconductor photocatalysis has attracted increasing attention as a green technology to solve the current energy and environmental problems. In recent years we have witnessed the renewed appeal of harvesting and the direct conversion of solar energy into chemical energy by utilizing the sunlight-driven photocatalysts. Although heterogeneous photocatalysts are almost exclusively semiconductors, more recently the plasmonic noble metals (typically gold and silver) have played an important role in the field of photo-driven chemical conversion due to their surface plasmon resonance (SPR). For example, the pioneering work of Awazu and co-workers introduced the concept of SPR into the field of photocatalysts, that is plasmonic photocatalysts[1]. Since the first report on the visible-light Ag@AgCl plasmonic photocatalysts by research group of Huang in 2008[2], a large number of Ag@AgX (X=Cl, Br, I) plasmonic photocatalysts have attracted much attention. Up to now, various sizes and structures of the new family have been fabricated, which include nanocubic[3, 4], near-spherical[5, 6], rounded triangular pyramid[7], polyhedral[8], heart-like[9], nanocashew[10], hollow-sphere micro/nanostructure[11], etc. In those cases, plasmonic nanostructures have been synthesized via either hydrothermal, ion-exchange method or direct precipitation process, where a subsequent light-, microwave- or heat-induced generation of Ag is required. Similar to the traditional photocatalysts, the quality and morphology of Ag@AgX (X=Cl, Br, I) influence importantly on their photocatalytic activity. Several micrometers sized Ag@AgX cause the recombination of the plasmon-induced electron-hole pairs before they arrive at the photocatalyst surface. The efficient separation of electron-hole pairs is critical for an enhanced plasmonic photocatalyst system. Therefore, owing to their morphology-dependence, one-step synthesis of the metal-semiconductor photocatalysts with high quality and activity is desirable.

To modulate the quality and morphology of plasmonic photocatalysts, since the report on tailoring nanoscale materials and composites using various amphiphilic molecules[12], surfactant-based composite systems have been harnessed again recently [4, 11, 13-18]. Shape-directing surfactants or specific surface capping agents such as polyvinyl pyrrolidone (PVP), cetyltriethylammonium bromide (CTAB) and cetyltrimethylammonium chloride (CTAC) were needed to guide the formation or induce anisotropic growth of different Ag@AgX (X=Cl, Br, I) that are usually synthesized via water/oil or oil/water microemulsions. However, the presence of large amounts of these agents leads to a decrease of active sites, which severely affect their photocatalytic activity[15]. Therefore, it is a big challenge to develop the morphology-controlled photocatalysts with “clean” surface structure without adding any capping agent. The emergence of single-layer graphene oxide (GO) has received extensive attention and shows great potential as an ideal additive

for controlling the formation of inorganic single crystals owing to its unique two-dimensional (2D) nanostructure, good flexibility and abundant functional groups on its surface [14, 19-21]. As an attractive precursor of graphene, the intrinsic hydroxyl, epoxy and carboxylic functional groups could act as active anchoring sites for the heterogeneous nucleation of metal ions such as Au^{3+}, Ag^{+}, Ti^{3+}, Zn^{2+}, Ca^{2+}, etc. In particular, its large surface and tunable surface properties allow it to be a competitive host substrate for the heterogeneous growth of desired guest materials. Furthermore, the competitive growth of nucleated clusters on GO surface may tailor the size and microstructure of the final particles. For example, very recently, by using monolayer GO sheets as a synthetic template, Huang et al. synthesized exquisite square-like Au nanosheets, which exhibited an edge length of 200-500 nm and a thickness of ~2.4 nm[19]. Composite crystals of calcium carbonate ($CaCO_3$)/graphene with hexagonal plate, dendritic and rhombohidral shapes were synthesized using GO sheets as the template to precisely control the mineralization process of $CaCO_3$[14]. Mesoporous anatase TiO_2 nanospheres/graphene composite photocatalysts by template-free self-assembly were presented, in which the final size and microstructure of TiO_2 could be tailored by the graphene sheets[22]. However, no work related to morphology-controlled plasmonic photocatalysts with GO as the template has been reported. Hence, the development of graphene-based plasmonic photocatalyst system is of fundamental and practical significance.

In this paper, we report our new efforts to synthesize the Ag@AgX@Graphene (X=Cl, Br) nanocomposites, where an accelerated GO reduction and generation of Ag nanocrystals occurred simultaneously by photoreducing AgX@GO nanocomposites. Interestingly, the cubic Ag@AgCl and quasi-cubic Ag@AgBr nanoparticles were manipulated by the orientation growth of AgX nanoparticles on the amphiphilic GO template. The obtained hetero-products display enhanced plasmonic photocatalytic activity and good recycling stability toward acridine orange (AO) pollutant under sunlight irradiation, which is ascribed to the synergistic effect of strong SPR excited by Ag nanocrystals and the conductive graphene sheets network for rapid carrier transfer and export between two components in the composite system. It is anticipated to open new possibilities in the application of graphene-based composites as the photocatalysis in environment remediation.

Experimental

Materials

Purified natural graphite (SP-1) was purchased from Bay Carbon, Inc., Michigan, USA. Other chemicals unless noted were from Wako Pure Chemical Industries, Ltd., or Sigma–Aldrich Inc., Japan.

Preparation of GO aqueous solution

GO was obtained from natural graphite, based on the method proposed by Hummers and Offeman, as reported previously by our group[23]. In a typical treatment, 5 g of the expanded graphite was dispersed in 115 mL concentrated sulfuric acid in an ice bath. Approximately 5 g sodium nitrate and 15 g potassium permanganate were slowly added to the chilled mixture, cooled by an ice bath, and stirring was continued for 2 hours. The mixture gradually became pasty and blackish-green. Then, the mixture was placed in a 35 °C water bath and kept at that temperature for 30 min, followed by the slow addition of distilled water (500 mL) to keep the solution from effervescing. The resulting solution was placed at well below 98 °C for 2 hours. As the reaction progressed, the color of the mixture turned yellowish. The mixture was further treated with 5% H_2O_2 (200 mL), filtered and washed with distilled water several times until its supernatant was without SO_4^{2-}, as tested by barium chloride solution (0.2 mM). The purified GO was finally dispersed in water and ultrasonically exfoliated in an ultrasonic bath for 1 hours to form a stable GO aqueous dispersion.

Synthesis of Ag@AgX, Ag@AgX@GO and Ag@AgX@Graphene

In a typical process, 10 mL aqueous solution of GO sheets (1 mg mL^{-1}) was added into 100 mL of ammonia-silver solution (with silver ions concentration of 10 mmol L^{-1}) under vigorous magnetic stirring for 1 hour. Then, 10 mL NaCl (or NaBr) solution (0.1 M) was added dropwise into the above solution successively within 10 min under magnetic stirring. The vigorous stirring was maintained for 24 hours under ambient conditions to form a light brown homogeneous suspension. The opaque suspension was mixed with 20 mL methanol and irradiated under the UV light (100 W, 365 nm, UVP B-100A). A dark brown suspension was obtained soon. Finally, the suspension was treated by centrifugation (10000 rpm, 10 min), and the produced solids were collected, washed thoroughly with deionized water and dried in 50 °C. In the control experiment, the corresponding Ag@AgX nanospecies were also synthesized via a parallel process without GO sheets. Ag@AgX@GO nanocomposites were also synthesized via a parallel process without UV-irradiated reduction. Note that the abovementioned synthesis works were performed without being protected from ambient light.

Photocatalytic performance

For the photocatalytic degradation experiments that used sunlight as energy source, a photocatalyst sample typically containing 10 mg of the loaded catalysts was dispersed in a 30 mL aqueous solution of AO dye (20 mg L^{-1}) and the illumination intensity of sunlight was 80 mW cm^{-2} to make the experimental results reasonably comparable with those obtained previously. The dispersion was kept in the dark for 60 min for dark adsorption experiment, after which the photodegradation was carried out. The dark adsorption was designed to be 60 min because the adsorption results indicated AO molecules was absorbed to saturation on the surface of catalysts (data not shown). At certain time intervals of sunlight irradiation, reaction solution was taken out from the system for the real-time investigation. The concentration of AO dye was monitored by UV-vis spectroscopy through recording the absorbance of the characteristic peak of AO at 490 nm. For the evaluation of the photocatalytic activity, *C* is

This journal is © The Royal Society of Chemistry [year]

the concentration of AO molecules at a real-time *t*, and C_0 is that in the AO solution immediately before it was kept in the dark. For comparison, blank experiment without photocatalysts has also been carried out.

Photoelectrochemical test

The photocurrent response tests were measured using electrochemical analyzer (ALS/CH Instruments 852C, ALS) in a standard three-electrode system using the as-prepared samples as the working electrodes with a diameter of ~3 mm, a platinum electrode as the counter electrode, and Ag/AgCl as the reference electrode. 1M Na_2SO_4 aqueous solution was used as the electrolyte. For the working electrodes, 20 mg catalyst was suspended in 1 mL nafion aqueous solution (2 wt %), the mixtures were ultrasonicated for 15 min to disperse it evenly to get a slurry. The slurry was coated onto the glass carbon electrode and dried under ambient conditions. The current-time (*i-t*) curves were collected at 1.0 V *vs* Ag/AgCl reference electrode. The intensity of sunlight irradiation was 80 mW cm^{-2} using super solar simulator with one-sun irradiation.

Characterizations

The morphological observations were carried out using scanning electron microscopy (SEM, JSM-6390, JEOL Co., Japan) and high resolution transmission electron microscopy (HR-TEM, HD-2000, Hitachi Co., Tokyo, Japan). Atomic force microscopy (AFM) images were acquired using an Agilent Series 5500 AFM instrument. The samples were prepared by casting a highly diluted GO aqueous suspension on the surface of mica. The images were obtained using the tapping mode at a scanning rate of 0.5 Hz. The X-ray diffraction (XRD) measurements were performed with a Rigaku RINT Ultima diffractometer with Cu-Kα radiation (Kα 1.54056 Å) and an X-ray power of 40 kV/20 mA at a scan rate of 4º min^{-1}. Fourier transform infrared spectroscopy (FT-IR) was performed over the wave number range of 4000–400 cm^{-1} with a FT/IR-6100 FT-IR Spectrometer, (JASCO, Japan). The X-ray photoelectron spectroscopy (XPS, JPC-9010MC, JOEL, Japan) analysis was performed by using an unmonochromated Mg-Kα X-ray source (1253.6 eV) with vacuum better than 1×10^{-7} Torr. For the transmission electron microscopic (TEM) analysis, the samples were suspended in water/menthol (0.2 mg mL^{-1}) by ultra-sonication for 10 min and then the dispersion was drop-casted on a fresh lacey carbon TEM grid. The beam energy used for TEM analysis was 200 keV. Raman analysis was performed with Invia Raman Microscope (Renishaw, United Kingdom) with an excitation wavelength at 532 nm. The photocatalytic performance of the samples under sunlight were evaluated by the degradation of AO dye under super solar simulator with one-sun irradiation (Super Solar Simulator, WXS-156S-L2, AM 1.5GMM, Wacom Electric. Co., LTD.).

Results and discussion

Typically, quasi-spherical Ag@AgCl and Ag@AgBr could be facilely fabricated by adding an aqueous solution of NaCl into a solution of $[Ag(NH_3)_2]OH \cdot xH_2O$. Cubic Ag@AgCl@Graphene and quasi-cubic Ag@AgBr@Graphene could also be produced via a similar process when a GO aqueous solution was added to the system prior to the addition of NaCl solution. The hydroxyl, epoxide and carboxylic functional groups on GO sheets could act as favorable anchoring sites for the heterogeneous nucleation and hetero-growth of AgX nanoparticles. During the growth process, few amount of Ag^+ in AgX are converted into Ag nanocrystals by the ambient light. Whereas under the subsequent UV irradiation, more Ag^+ are converted, simultaneously with the enhanced reduction efficiency of the adjacent GO into graphene within fewer hours, compared with the previous research[24]. Experimentally, an opaque suspension with a light brown was obtained soon after the dropwise addition of the NaCl solution into the aqueous solution of $[Ag(NH_3)_2]OH \cdot xH_2O$ and then a much darker brown suspension was obtained after UV irradiation

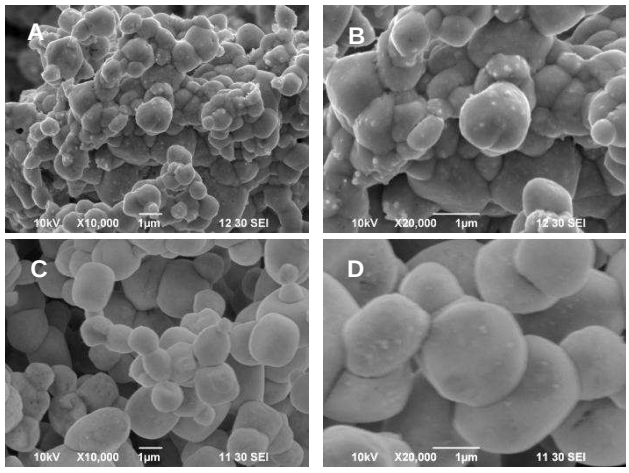


Fig. 1 Quasi-spherical Ag@AgCl (A and B) and Ag@AgBr (C and D) photocatalysts with inhomogenous particle size.

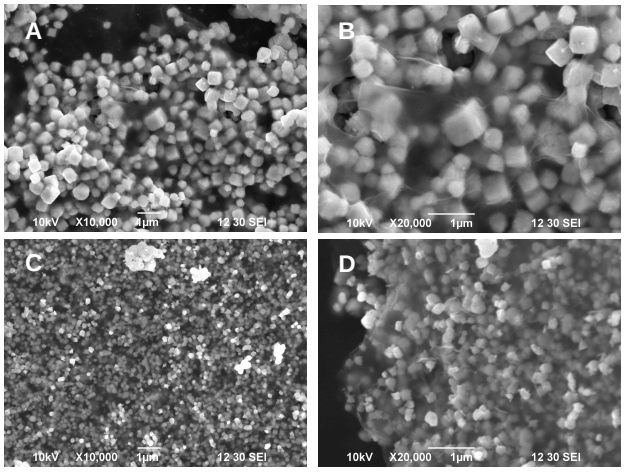


Fig. 2 Representative SEM images of the as-prepared cubic Ag@AgCl and quasi-cubic Ag@AgBr nanoparticles encapsulated by gauze-like graphene sheets in Ag@AgCl@Graphene (A and B) and Ag@AgBr@Graphene (C and D), respectively.

(ESI, Fig. S1). The morphologies of as-synthetized nanostructures are characterized by scanning electron microscopy

(SEM), as shown in Fig. 1 and Fig. 2. The Ag@AgCl and Ag@AgBr samples exhibit quasi-spherical structures with sizes of 0.8~1.5 μm as reported previously [2, 25, 26]. While after involving the multifunctional GO, the cubic Ag@AgCl and quasi-cubic Ag@AgBr nanostructures with an average edge length of 400 nm and 200 nm, respectively, were manufactured without the addition of any other surfactant. After photoreduction, the as-prepared Ag@AgX nanoparticles are distinctly enwrapped with gauze-like graphene sheets, which significantly improve the dispersibility and homogeneity of Ag@AgX. On the other hand, by functioning as "spacer", these cubic-like nanoparticles attached onto graphene sheets can prevent graphene sheets from aggregation and restacking, and both of the two faces of graphene sheets are accessible in their application. The transparent gauze-like structure with well restored conjugated networks of the graphene sheets were maintained in the final products, which could promote electron transfer of the catalysts in photocatalytic

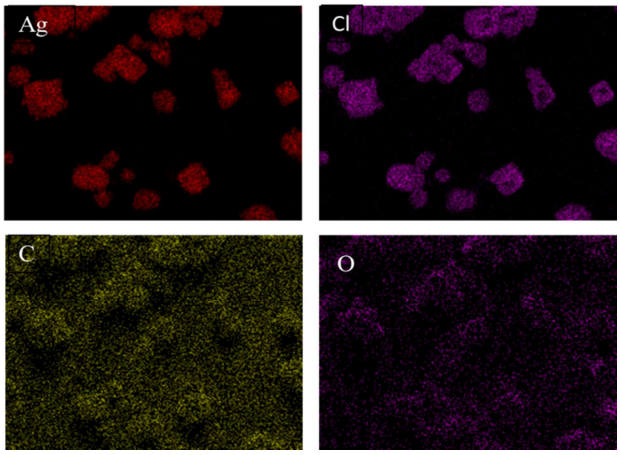


Fig. 3 Represent EDX mapping images of Ag@AgCl@Graphene nanocomposites.

reaction and favorably improve the adsorption capacity of Ag@AgX@Graphene due to its high surface area. The ordered structure of the as-prepared Ag@AgX@Graphene compared with the bare Ag@AgX could be attributed to the existence of GO sheets, which play a role as a template modulating the growth of Ag@AgX crystals along certain directions, resulting in a smaller sized of cubic-like products. It has been verified that the multifunctional GO sheets, which could physicochemically and structurally be regarded as an unconventional amphiphilic surfactant[16]. In that case, GO sheets can work as capping agent or stabilizer to hamper the growth of nanoparticles randomly, which affect the morphology and size of the resultant nanoparticles[4, 18, 27]. The exact role of GO sheets in this process and the formation mechanism of the as-prepared crystals remain to be further studied and established. A representative TEM image of the Ag@AgCl@Graphene nanocomposites further confirmes the cubic nanoparticles were uniformly attached to the surface of gauze-like graphene sheets (ESI, Fig. S2). The full potential of graphene in Ag@AgCl@Graphene is released to the maximum for which the presence form of graphene sheets remains at a single or few layers. Furthermore, the EDX mapping images of Ag@AgCl@Graphene is demonstrated to illustrate the distribution of C, O, Cl and Ag elements (Fig. 3). Unfortunately, high-resolution TEM image of Ag@AgX@Graphene was not obtained because these nanoparticles were destroyed by the high-energy electron beam during the measurement.

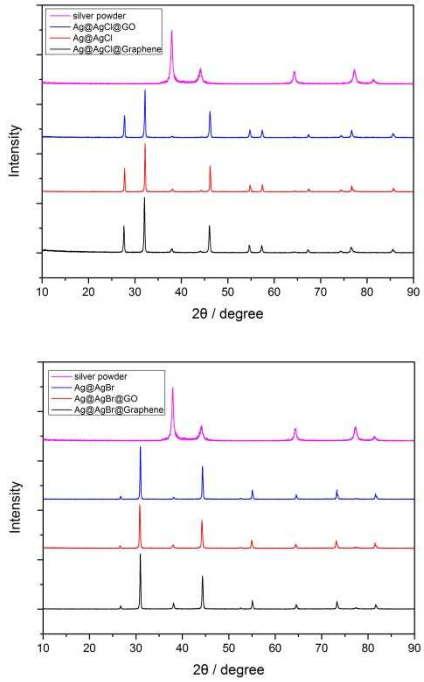


Fig. 4 XRD spectra of the standard silver powder, bare Ag@AgX, Ag@AgX@GO and the quasi-cubic Ag@AgX@Graphene nanocomposites.

The crystal structures of the obtained Ag@AgX@Graphene (X=Cl, Br) plasmonic photocatalysts are characterized by X-ray diffraction (XRD). As shown in Fig. 4, the crystalline phase of standard silver powder, bare quasi-spherical Ag@AgCl, Ag@AgCl@GO and cubic Ag@AgCl@Graphene were investigated. The XRD patterns display distinct diffraction peaks (2θ) at 38.2 (111), 44.6 (200), 67.4 (400), 74.4 (331), 85.6 (422), respectively, which correspond to the typical cubic phase of standard metallic Ag and that of AgCl (JCPDS file: 31-1238). Due to the high photosensitivity of bare AgX, Ag nanocrystals aggregate on the surface of AgX under the ambient light in the cases of Ag@AgX@GO. Compared with Ag@AgX and Ag@AgX@GO, the peak intensity of Ag@AgX@Graphene shows stronger, indicating that simultaneously with the reduction of GO into graphene under UV irradiation more Ag nanocrystals generate, which can be confirmed below by the XPS. These results verify the evident interactions between the generation of Ag nanocrystals and the reduction of GO, as also suggested by other researchers[28].

To investigate the morphology evolution of Ag@AgX@Graphene nanocomposites, the growth process of representative Ag@AgCl@Graphene was further studied by analyzing two intermediate stages as indicated in Fig. 5. In the first stage, a large amount of irregular AgCl seeds with varying sizes were formed during the initial 4 hours. Due to the

This journal is © The Royal Society of Chemistry [year]

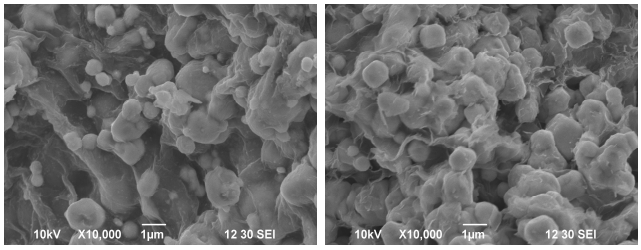


Fig. 5 SEM images of the shape evolution of the representative Ag@AgCl@GO samples obtained at different reaction stages: the formed quasi-spherical Ag@AgCl@GO seeds after 4 hours (left) and a certain number of quasi-spherical Ag@AgCl@GO have been transformed into cubes after 12 hours (right).

complexation of functional oxygen-containning active sites anchoring with Ag^+, followed by the heterogeneous nucleation process accompanying the addition of chloridion, such a strategy could help put GO into full play with elaborate desigh, resulting in reinforced interfacial contact between GO and AgCl nanoparticles[29]. After 12 hours, the AgCl nanoparticles encapsulated tightly by GO tend toward uniformity with size of ~1 μm. Meanwhile, a certain amount of quasi-spherical AgCl particles were gradually transformed into AgCl cubes. When the reaction was performed for 24 hours, the as-prepared cubes were formed finally.

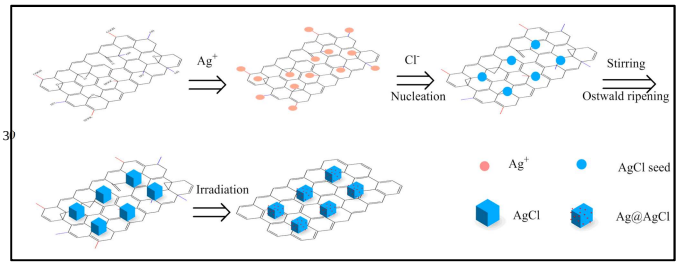


Fig. 6 Schematic Explanation for morphology evolution of the representative Ag@AgCl@Graphene nanocomposites.

On the basis of the above experimental observations, we proposed a possible fabrication strategy for the cubic Ag@AgCl@Graphene nanocomposites under ambient conditions (Fig. 6). Chemically derived GO, with a thickness of ~1.1 nm and size distribution on the order of micrometers (ESI, Fig. S3), carries abundant functional groups such as the hydroxyl, epoxide and carboxyl on the sheet surface. In GO solution, those active sites are leveraged to stabilize Ag^+ and subsequently grown to the initial AgCl seeds via the seeding growth mechanism. As the time progresses, the functional layered sheets play a role as surfactant template which makes the AgCl seeds grow along certain directions. For the face centered cubic (FCC) structure in particular, the crystal shape is determined mainly by the function of the ratio R, of the growth rate along the <100> to that of the <110> directions. For example, the cubes bounded by six equivalent {100} facets would form when R=0.58[30]. In this study, rapid nucleation occurred at a very early stage, producing a large amount of irregular AgCl seeds with varying sizes. These nucleis gradually grew along the controlled orientation to form the regular AgCl cubes in the presence of GO, while invariant shape in Ag@AgCl was obtained for comparison in the absence of GO, similarly reported by other researchers[4].

The chemical compositions and surface chemical states of the samples were further confirmed by X-ray photoelectron spectroscopy (XPS). As shown in Fig. 7, the C1s XPS spectrum for the Ag@AgCl@GO indicates a considerable degree of oxidation with four components that correspond to carbon atoms involved in different functional groups, namely, the non-oxygenated aromatic C (C=C/C-C), the C in C-O bonds, the carbonyl C (C=O) and the carboxylate C (-COO-), centered around the binding energies of 284.3, 286.2, 288.1, and 290.1 eV, respectively. After the UV irradiation, the intensities for all C1s peaks of the carbon-oxygen binding species, especially the peaks of C-O and C=O bonds decreased rapidly, revealing that most of the oxygen containing functional groups were removed in the Ag@AgCl@Graphene system after photoreduction; the C/O ratio increased from 2.37:1 to 4.83:1. While for the

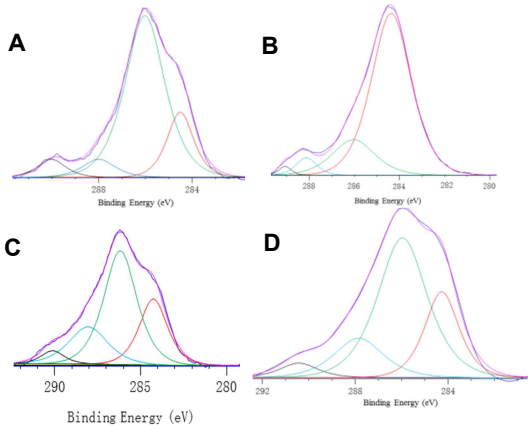


Fig. 7 C1s XPS spectra of (A) Ag@AgCl@GO, (B) Ag@AgCl@Graphene, (C) Ag@AgBr@GO and (D) Ag@AgBr@Graphene nanocomposites.

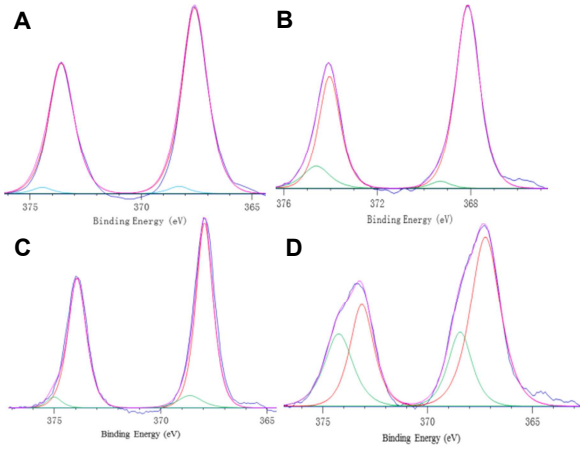


Fig. 8 XPS spectra of Ag 3d of (A) bare Ag@AgCl, (B) Ag@AgCl@Graphene nanocomposites and (C) bare Ag@AgBr, (D) Ag@AgBr@Graphene nanocomposites.

Ag@AgBr@Graphene system, the C/O ratio increased from 2.49:1 to 4.19:1. In previous studies, the C/O ratio for graphene obtained by using UV irradiation of GO aqueous solution was

increased from 2.20:1 to 5.90:1. However, the reduction process required over 16 hours under 300 W ultraviolet light[28]. It is true that the reduction rate was accelerated in our system, which could facilitate the charge transfer from Ag@AgX to the surface of graphene. Simultaneously, more Ag nanocrystals were obtained with the photoreduction of GO under UV irradiation, which is also confirmed by the XPS spectra of Ag 3d (Fig. 8). For the bare Ag@AgX samples, two bands at 367.5 and 373.6 eV corresponding to the binding energies of Ag $3d_{5/2}$ and Ag $3d_{3/2}$, respectively, are observed. These two bands could be further divided into two groups of peaks 367.5, 368.4 eV and 373.6, 374.3 eV, where the peaks at 367.5 and 373.6 eV are attributed to Ag^+ in AgX, whereas those at 368.4 and 374.3 eV are attributed to the Ag nanocrystals. The calculated surface mole ratio of the Ag nanocrystals to Ag^+ for Ag@AgCl and Ag@AgBr is ca. 1:24 and 1:13, respectively. In the cases of graphene-involved Ag@AgX@Graphene nanocomposites, the Ag $3d_{5/2}$ and Ag $3d_{3/2}$ peaks shift to a higher binding energy to 368.2 and 374.1 eV, respectively. The two bands also yield four peaks at 368.2, 369.2 eV and 374.1, 374.8 eV, respectively. The peaks at 368.2 and 374.1 eV could be ascribed to Ag^+, and those at 369.2 and 374.8 eV are attributed to the Ag nanocrystals. It is interesting that compared with the bare Ag@AgX, these peaks shift to higher binding energies in Ag@AgX@Graphene with a value of ca. 0.6 eV. In addition, the calculated surface mole ratio of the Ag nanocrystals to Ag^+ for Ag@AgCl@Graphene and Ag@AgBr@Graphene increases distinctly to ca. 1:10 and 1:4, respectively. In the XPS spectra of Cl 2p and Br 3d of the samples (ESI, Fig. S4), the observed peak could be fitted with two peaks corresponding to Cl 2p3 (197.7 eV), Cl 2p1 (199.5 eV) and Br $3d_{5/2}$ (67.8 eV), Br $3d_{3/2}$ (68.8 eV), respectively, in good agreement with that of AgCl[11] and AgBr[31].

The formation of Ag@AgX@Graphene nanocomposites by photoreduction in our system can be explained based on the following proposed mechanism. The first step involves the heterogeneous nucleation process of AgX seeds on the surface of GO via the electrostatic interaction between Ag^+ and negatively charged groups on GO surface. Then, the AgX nanoparticles undergo an orientation growth whose surface is encapsulated with functional GO. Subsequently, the AgX nanoparticles would decompose and generate more Ag^0 species through photosensitization under the UV irradiation. The Ag nanocrystals are produced depending on the aggregation of the Ag^0 species and deposited on the surface of AgX nanoparticles. Owing to the excitation by UV irradiation, the Ag nanocrystals photogenerate electrons and holes. Then, the plasmon-induced electrons are injected into the conduction band of adjacent GO, thus causing the reduction of GO, while the produced positive holes are scavenged by methanol. A similar photoreduction mechanism has been observed in the Ag/GO[28] and Ag/TiO_2/GO systems[32]. It is demonstrated that the generation of Ag nanocrystals and the reduction of GO occur in the interactive process. Due to the presence of GO, more Ag nanocrystals can be formed in the Ag@AgX@Graphene system than those without GO sheets, as confirmed by the XPS spectra of Ag 3d. The related reactions are as follows:

$$AgCl \xrightarrow{h\nu} Ag^0 + \frac{1}{2}Cl_2$$

$$nAg^0 \rightarrow Ag_n \quad (Ag_n\text{: Ag nanocrystals})$$

$$Ag_n \xrightarrow{h\nu} e^- + hole^+$$

$$GO + e^- \rightarrow Graphene$$

To validate the synergistic effect between the Ag@AgX nanoparticles and graphene sheets, the Fourier transform infrared spectrum (FT-IR) of the samples together with that of the original GO and reduced graphene oxide (RGO) with green reductant thiourea dioxide (TDO) as reported previously by our group were investigated. As seen in Fig. 9, the carbonyl stretching band at 1728 cm^{-1} exhibited by the original GO and RGO, shifts to a lower wavenumber, 1716 cm^{-1} and 1710 cm^{-1} for the graphene in Ag@AgCl@Graphene and Ag@AgBr@Graphene, respectively. This result verifies the evident interactions between Ag@AgX and graphene sheets, further suggesting the successful hybridization between these two components[18, 33].

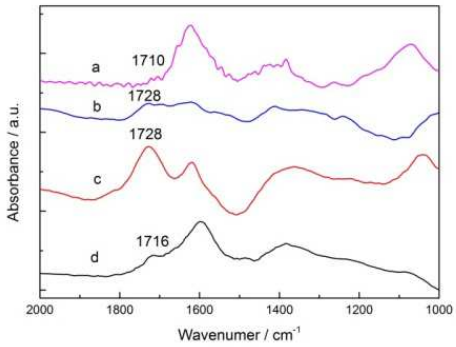


Fig. 9 FT-IR spectra of (a) Ag@AgBr@Graphene nanocomposites, (b) RGO, (c) GO and (d) Ag@AgCl@Graphene nanocomposites.

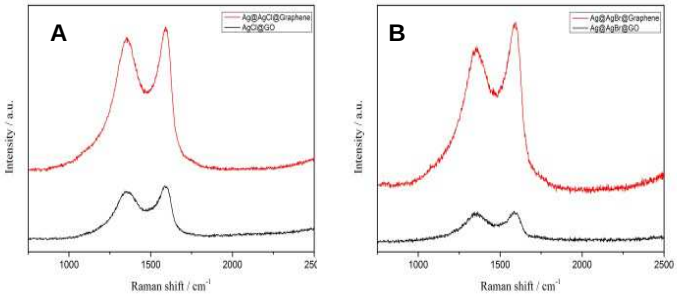


Fig. 10 Raman spectra of (A) Ag@AgCl@GO, Ag@AgCl@Graphene and (B) Ag@AgBr@GO, Ag@AgBr@Graphene nanocomposites.

Furthermore, the structural change and the interaction effect between them could also be disclosed by the Raman spectra, as shown in Fig. 10. Two characteristic peaks of the graphitic material, namely D and G band, were also observed in Ag@AgX@GO and Ag@AgX@Graphene around 1350 cm^{-1} and 1590 cm^{-1}, respectively. They are attributed to the breathing mode of κ-point phonons of A_{1g} symmetry and the first order scattering of E_{2g} vibration mode of sp^2-bonded carbon atoms. Interestingly, the two bands intensity are significantly enhanced by approximately 3.80 and 5.40 folds in Ag@AgCl@Graphene

This journal is © The Royal Society of Chemistry [year]

and Ag@AgBr@Graphene after photoreduction. The strong Raman signal enhancement that similar to the surface enhanced Raman scattering (SERS) could be attributed to the SPR field induced by Ag nanocrystals in Ag@AgX@Graphene nanocomposites[34]. These results further confirm the occurrence of efficient charge transfer between Ag@AgX and graphene sheets of our graphene-involved nanocomposites, where Ag@AgX and graphene sheets work as electron donor and electron acceptor, respectively. In addition, the intensity ratio of D-band to G-band (I_D/I_G) in the Raman spectrum increased from 2.33 for Ag@AgCl@GO to 3.73 in the photoreduced Ag@AgCl@Graphene, while that from 2.36 for Ag@AgBr@GO to 2.99 in Ag@AgBr@Graphene, indicating a decrease in the average size of the in-plane sp^2 domains of C atoms in the as-prepared Ag@AgX@Graphene nanocomposites, which is similar to that observed in the chemical reduced graphene[35].

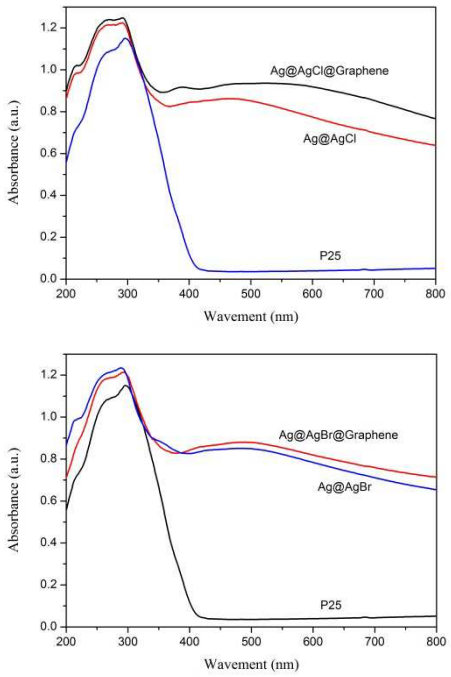


Fig. 11 UV-vis diffusive reflection spectra of P25 (TiO_2), Ag@AgX and Ag@AgX@Graphene nanocomposites.

For sunlight energized photocatalysts, it is required that they could display distinct absorption in the visible region. The optical properties of plasmonic noble metal are dominated by their SPR when excited by incident light with a specified wavelength. The SPR could interact with the metal particles to establish the photon-stimulated collective oscillations of the conduction band electrons, which occurs with an exciting way of including light absorption in visible, infrared (IR) and NIR regions. As shown in Fig. 11, the UV-visible diffuse reflection spectra of the synthesized Ag@AgX and Ag@AgX@Graphene exhibit distinct absorption both in the UV and visible regions. The commercially available TiO_2 (P25) is also employed as the reference photocatalyst. It can be seen that distinct absorption could be detected in the UV region, while negligible absorption could be observed in the visible region. In the cases of as-prepared Ag@AgX and Ag@AgX@Graphene, broad and strong absorption both in UV and visible regions could be distinctly detected. Generally, bare AgX could only show apparent absorption in the UV region but negligible absorption in the visible region. This also suggests the existence of Ag nanocrystals in Ag@AgX and Ag@AgX@Graphene, which could arouse plasmonic resonance absorption in the visible region. Moreover, the obtained Ag@AgX@Graphene exhibit stronger absorption toward the visible light than their corresponding Ag@AgX@GO precursors without shifted absorption edge. Accordingly, these results further confirm that there indeed exist the synergistic effect between the Ag@AgX component and graphene sheets, as confirmed by the above FT-IR observation.

To investigate the plasmonic photocatalytic activity of the Ag@AgX@Graphene nanocomposites, the photodegradation of AO dye was carried out under sunlight irradiation. Experimentally, 10 mg of the loaded catalysts was suspended in 30 mL AO solution (20 mg L^{-1}) and the intensity of sunlight was 80 mW cm^{-2} to make the experimental results reasonably comparable with those obtained previously. As it is known, the adsorptive ability of photocatalyst for the pollutant molecules is one of the crucial factors to enhance the catalytic property[36, 37]. Dark adsorption experiments were carried out for 60 min to achieve the equilibrium prior to the sunlight irradiation. The graphene-involved samples display a distinctly higher adsorptivity for AO than the bare Ag@AgX and P25, which is beneficial for enhancing their photocatalytic activity. The adsorptivity was enhanced ~20%, which can be seen from the Figure. This could be ascribed to the hybridization of graphene sheets, which has been proven to facilitate the adsorption, owing to the noncovalent intermolecular π-π interactions between pollutant molecules and the large graphene sheets area[18, 37, 38]. The normalized temporal concentration changes of AO during the photodegradation process under sunlight irradiation are shown in Fig. 12. In the blank experiment where no catalysts were employed, negligible photodegradation of the AO was observed, indicating the self-photosensitized decomposition of AO could basically be ignored under our experimental conditions. When the bare Ag@AgX samples were used as photocatalysts, 65% of the AO were decomposed after 25 min. In contrast, when Ag@AgCl@Graphene and Ag@AgBr@Graphene were employed, an approximate 95% and 92% of the AO were decomposed, respectively. It demonstrates that graphene-involved Ag@AgX@Graphene nanocomposites have much higher photocatalytic activity than the bare Ag@AgX. Multifactors, such as the higher adsorptive capacity, the smaller size of Ag@AgX and the reinforced electron-hole pair separation owing to the interfacial contact between Ag@AgX and graphene sheets components, resulting in an enhanced photocatalytic decomposition performance[4, 18, 29]. It has been proven that both for the bare Ag@AgCl and the Ag@AgCl@GO nanocomposites, the cubic-like nanospecies display higher photocatalytic performance than those of the corresponding sphere-like nanostructures under sunlight irradiation[4]. Accordingly, an interesting morphology dependent and enhanced photocatalytic activity could be easily achieved in our system. Moreover, the photocatalytic stability of Ag@AgX@Graphene nanocomposites were also evaluated by the repeated photodegradation of AO, as

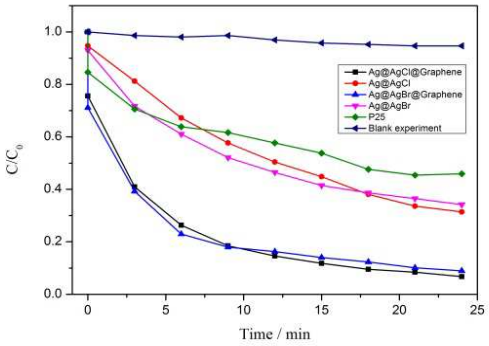


Fig. 12 Photocatalytic performance of the thus-prepared Ag@AgX@Graphene plasmonic photocatalysts for the degradation of AO pollutant under sunlight irradiation.

those in previous work[2, 11, 25]. After five times recycling experiments, only slight decrease was observed, indicating the good photocatalytic stability (data not shown). The slight decrease of the activities could be attributed to the loss of the catalysts in every recycling process. These results suggest that Ag@AgX@Graphene nanocomposites are stable under sunlight irradiation and very promising in practical application.

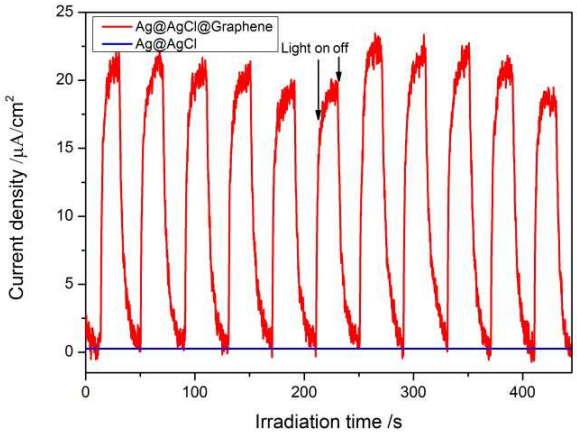


Fig. 13 Photocurrent response of Ag@AgCl and Ag@AgCl@Graphene nanocomposites in 1M Na_2SO_4 aqueous solution under sunlight irradiation at 1.0 V vs. Ag/AgCl reference electrode.

Furthermore, to confirm the above proposed electron-hole pairs separation in the photocatalytic degradation process, the transient photocurrent response of Ag@AgCl and graphene involved Ag@AgCl@Graphene photocatalysts were recorded as shown in Fig. 13. Several on-off cycles via intermittent sunlight irradiation were performed. The photocurrent value of Ag@AgCl@Graphene increased rapidly to a comparatively constant value when the light was on, and the photocurrent value decreased gradually to zero when the light was off. In constant, there scarcely existed any photocurrent density for Ag@AgCl sample. The involvement of graphene supply transport channels for the photogenerated electrons from conduction band of AgCl semiconductor, leading to the gradual decrease of photocurrent to zero. In addition, the fast photoresponse features also exhibited a good reproducibility during the repeated on-off cycles. Based on the above results, the proposed fabrication of heterogeneous components consisting Ag@AgCl and gauze-like graphene sheets is a feasible strategy to develop active photocatalysts under sunlight irradiation.

Conclusions

We have demonstrated that two kinds of novel Ag@AgX@Graphene heterostructures with high sunlight-driven plasmonic photocatalysis and excellent stability, which could be facilely produced by photoreducing their corresponding AgX@GO precursors under ambient conditions. Unlike the bare spherical Ag@AgX, cubic Ag@AgCl and quasi-cubic Ag@AgBr nanoparticles encapsulated by graphene sheets network are manipulated by controlling the selective orientation growth of AgX nanoparticles through the abundant active sites on two-dimensional GO sheets, where they function as amphiphilic template. With the unique structure, these nanocomposites could be employed as plasmonic photocatalysts for the efficient decomposition of AO molecules under sunlight irradiation. The graphene-involved Ag@AgX@Graphene nanocomposites have much higher photocatalytic performance than the bare Ag@AgX samples. This study provides a new avenue for the assembly of morphology-controlled plasmonic photocatalysts that utilize sunlight as an energy source in the application of environment remediation.

Notes and references

Laboratory of Environmental Remediation/Nano-Technology Industrialization, Graduate School of Environmental Science, Hokkaido University, Kita8, Nishi4, KitaKu, Sapporo 001-0021, Hokkaido, Japan. Fax:+81 011-706-9294; Tel: +81 011-706-9235; E-mail: wang2011@ees.hokudai.ac.jp

† Electronic Supplementary Information (ESI) available: [details of any supplementary information available should be included here]. See DOI: 10.1039/b000000x/

1. K. Awazu, M. Fujimaki, C. Rockstuhl, J. Tominaga, H. Murakami, Y. Ohki, N. Yoshida and T. Watanabe, *J. Am. Chem. Soc.* , 2008, **130**, 1676.
2. P. Wang, B. Huang, X. Qin, X. Zhang, Y. Dai, J. Wei and M.-H. Whangbo, *Angew. Chem. Int. Ed.* , 2008, **47**, 7931.
3. C. An, S. Peng and Y. Sun, *Adv. Mater.* , 2010, **22**, 2570.
4. M. Zhu, P. Chen and M. Liu, *J. Mater. Chem.* , 2011, **21**, 16413.
5. Z. Lou, B. Huang, X. Qin, X. Zhang, Z. Wang, Z. Zheng, H. Cheng, P. Wang and Y. Dai, *Crystengcomm*, 2011, **13**, 1789.
6. Z. Lou, B. Huang, P. Wang, Z. Wang, X. Qin, X. Zhang, H. Cheng, Z. Zheng and Y. Dai, *Dalton Trans.* , 2011, **40**, 4104.
7. J. Jiang and L. Zhang, *Chem. Eur. J.* , 2011, **17**, 3710.
8. H. Wang, X. Lang, J. Gao, W. Liu, D. Wu, Y. Wu, L. Guo and J. Li, *Chem. Eur. J.* , 2012, **18**, 4620.
9. J. Liao, K. Zhang, L. Wang, W. Wang, Y. Wang, J. Xiao and L. Yu, *Mater. Lett.* , 2012, **83**, 136.
10. C. An, J. Wang, C. Qin, W. Jiang, S. Wang, Y. Li and Q. Zhang, *J.*

This journal is © The Royal Society of Chemistry [year]

Mater. Chem. , 2012, **22**, 13153.
11. P. Wang, B. Huang, Z. Lou, X. Zhang, X. Qin, Y. Dai, Z. Zheng and X. Wang, *Chem. Eur. J.* , 2010, **16**, 538.
12. J. Liu, A. Y. Kim, L. Q. Wang, B. J. Palmer, Y. L. Chen, P. Bruinsma, B. C. Bunker, G. J. Exarhos, G. L. Graff, P. C. Rieke, G. E. Fryxell, J. W. Virden, B. J. Tarasevich and L. A. Chick, *Adv. Colloid Interface Sci.* , 1996, **69**, 131.
13. Q. Xiang, J. Yu and M. Jaroniec, *Chem. Soc. Rev.* , 2012, **41**, 782.
14. X. Wang, H. Bai, Y. Jia, L. Zhi, L. Qu, Y. Xu, C. Li and G. Shi, *RSC Adv.* , 2012, **2**, 2154.
15. X. Chen, B. Su, G. Wu, C. J. Yang, Z. Zhuang, X. Wang and X. Chen, *J. Mater. Chem.* , 2012, **22**, 11284.
16. J. Kim, L. J. Cote, F. Kim, W. Yuan, K. R. Shull and J. Huang, *J. Am. Chem. Soc.* , 2010, **132**, 8180.
17. C. Xu, X. Wang, L. Yang and Y. Wu, *J. Solid State Chem.* , 2009, **182**, 2486.
18. M. Zhu, P. Chen and M. Liu, *ACS Nano*, 2011, **5**, 4529.
19. X. Huang, S. Li, Y. Huang, S. Wu, X. Zhou, S. Li, C. L. Gan, F. Boey, C. A. Mirkin and H. Zhang, *Nat. Commun.* , 2011, **2**, 292.
20. D. Li, M. B. Muller, S. Gilje, R. B. Kaner and G. G. Wallace, *Nat. Nanotechnol.* , 2008, **3**, 101.
21. X. Huang, X. Qi, F. Boey and H. Zhang, *Chem. Soc. Rev.* , 2012, **41**, 666.
22. N. Li, G. Liu, C. Zhen, F. Li, L. Zhang and H.-M. Cheng, *Adv. Funct. Mater.* , 2011, **21**, 1717.
23. B. Fugetsu, E. Sano, H. W. Yu, K. Mori and T. Tanaka, *Carbon*, 2010, **48**, 3340.
24. S. Pei and H.-M. Cheng, *Carbon*, 2012, **50**.
25. L. Kuai, B. Geng, X. Chen, Y. Zhao and Y. Luo, *Langmuir*, 2010, **26**, 18723.
26. H. Zhang, X. Fan, X. Quan, S. Chen and H. Yu, *Environ. Sci. Technol.* , 2011, **45**, 5731.
27. M. Zhu, P. Chen and M. Liu, *Langmuir*, 2012, **28**, 3385.
28. W. Wang, J. Cui, W. Fan, Z. Feng, X. Ma and W. Jiang, *Mater. Lett.* , 2012, **84**, 120.
29. N. Zhang, Y. Zhang and Y.-J. Xu, *Nanoscale*, 2012, **4**, 5792.
30. Z. L. Wang, *J. Phys. Chem. B*, 2000, **104**, 1153.
31. P. Wang, B. Huang, X. Qin, X. Zhang, Y. Dai and M.-H. Whangbo, *Inorg. Chem.* , 2009, **48**, 10697.
32. I. V. Lightcap, T. H. Kosel and P. V. Kamat, *Nano Lett.* , 2010, **10**, 577.
33. J. Petroski and M. A. El-Sayed, *J. Phys. Chem. A*, 2003, **107**, 8371.
34. DasA, PisanaS, ChakrabortyB, PiscanecS, S. K. Saha, U. V. Waghmare, K. S. Novoselov, H. R. Krishnamurthy, A. K. Geim, A. C. Ferrari and A. K. Sood, *Nat. Nanotechnol.* , 2008, **3**, 210.
35. F. Tuinstra and J. L. Koenig, *J. Chem. Phys.* , 1970, **53**, 1126.
36. W. Morales, M. Cason, O. Aina, N. R. de Tacconi and K. Rajeshwar, *J. Am. Chem. Soc.* , 2008, **130**, 6318.
37. H. Zhang, X. Lv, Y. Li, Y. Wang and J. Li, *ACS Nano*, 2010, **4**, 380.
38. J. Liu, H. Bai, Y. Wang, Z. Liu, X. Zhang and D. D. Sun, *Adv. Funct. Mater.* , 2010, **20**, 4175.